Rapid charge-transfer cascade through SWCNT composites enabling low-voltage losses for perovskite solar cells

Severin N. Habisreutinger[1]*, Nakita K. Noel[2,3], Bryon W. Larson[1], Obadiah G. Reid[1,4], Jeffrey L. Blackburn[1]

[1] Chemistry and Nanoscience Center, National Renewable Energy Laboratory, 15013 Denver West Parkway, Golden, CO 80401, United States of America

[2] Department of Electrical Engineering, Princeton University, 41 Olden Street, Princeton, New Jersey 08544, United States of America

[3] Princeton Research Institute for the Science and Technology of Materials, Princeton University, 70 Prospect Ave, Princeton NJ, 08544, USA

[4] Renewable and Sustainable Energy Institute, University of Colorado at Boulder, Boulder, CO 80309, United States of America

Good charge selective contacts are vital to achieving efficient perovskite solar cells. The selectivity of such a contact is determined by its energetic offset or alignment with the bands of the perovskite absorber and, most importantly, by its low recombination losses.

In this study, we use single-walled carbon nanotubes (SWCNTs) as a high-mobility hole extraction layer at the interface with a perovskite absorber. When employed as a charge-transfer cascade-like structure with a low-mobility hole-selective contact, this configuration can suppress the interfacial recombination through the rapid removal of holes from the interface region. Reducing these recombination losses in turn results in very low voltage losses in full perovskite solar cells.

The rapid evolution of perovskite solar cells, from a curious off-shoot of dye-sensitized solar cells in 2009 to one of the most efficient thin-film technologies in photovoltaics in 2019, has been staggering.[1,2] Researchers in the field are now setting their sights on high-performance III-V semiconductors as a target for the performance potential of perovskite solar cells. One of the essential developments towards achieving comparable performances to the conventional III-V photovoltaics is to minimize the voltage loss, which is one of the main contributors to the inherent energy loss of a real photovoltaic device.

For perovskite-based devices, the issue of voltage loss can be addressed by either considering the absorber layer, the contacts, or both (the absorber/contact interface); recent literature reports have elucidated that the majority of losses occur at the perovskite interfaces where charge carriers are extracted.[3–5] Using absolute photoluminescence to investigate several of charge-selective layers (CTLs), Stolterfoht et al. demonstrate that the V_{OC} correlates with the radiative recombination

efficiency of the device stack.[6] The V_{OC} can thus be maximized when the non-radiative recombination at the interface is suppressed.[6] This can be achieved through two strategies: the reduction of the surface defect density and/or the increase in selectivity of the CTL. The former will largely depend on the quality of the perovskite surface, while the later will be determined by the properties of the CTL. Provided the junction between the perovskite and the CTL exhibits an appropriate energetic alignment or offset of the energy level, respectively, the selectivity of the CTL will depend on several parameters such as charge transfer kinetics, interfacial morphology, chemical interactions, interfacial dipoles, internal charge transport properties etc.[7] In this study, we intend to demonstrate that leveraging rapid charge transfer and high charge carrier kinetics within the HTL can be an effective approach to maximizing the selectivity of this contact, which in turn can translate into lower interfacial recombination and thus into a higher V_{OC}. We do this by exploring a model system of single walled carbon nanotube (SWCNT) embedded in hole-selective matrix.

SWCNTs are essentially rolled up sheets of graphene. These tubes can retain the excellent charge transport characteristics of graphene while confining the charge transport to a single dimension, thus facilitating highly directional charge transport with little resistance.[8] Since interactions with ambient oxygen typically result in a slight p-doping of the SWCNTs,[9] SWCNTs are commonly employed as p-type contact in perovskite solar cells.[10] In fact, the junction formed between SWCNTs and the perovskite absorber is therefore energetically and kinetically highly beneficial for hole extraction.[11,12] SWCNT networks have therefore been successfully employed as hole-extraction layers or contacts in perovskite solar cells.[10,13–15]

This study is a direct continuation of the previous studies which were proofs-of-principle in nature, demonstrating that a bi-layer structure of SWCNTs and a secondary matrix can yield efficiencies competitive to conventionally doped HTMs.[16,17] In this study, we investigate the details of the hole extraction of the composite structure, including SWCNTs embedded in a secondary matrix. We find that in devices the SWCNTs rapidly extract photogenerated holes from the perovskite, however, in order to prevent back-recombination at the SWCNT-perovskite interface, an additional secondary charge-selective material is required to remove the holes from the SWCNTs. Interestingly, the charge transport properties of the secondary material appear not to be limiting the device performance.

We demonstrate that the double-layer HTL is not the limiting factor with respect to the achievable voltage. We show this by reducing interfacial defects states on the perovskite absorber through a chemical intervention of the absorber layer which further improves the attainable open-circuit voltage. This finding demonstrates a strategy to improving the charge selectivity of a contact by enhancing the kinetics at the interface and, importantly, preventing interfacial recombination through removal of charges from the interface. Specifically, we demonstrate such a system using SWCNTs, known for their excellent charge transfer kinetics at the perovskite interface,[11,12] however, it is likely that this concept is generalizable to any system with a high-mobility interlayer which can improve the charge transfer at the interface with the perovskite, reduce recombination losses, and thus further improve the achievable photovoltage in perovskite solar cells.

The devices used in this work have a planar n-i-p architecture with a mixed A-site cation, lead,

mixed halide perovskite ($FA_{0.83}MA_{0.17}Pb(I_{0.83}Br_{0.17})_3$).[17] The interface of interest in this study is the interface between the perovskite absorber and the p-type contact. A thin layer of polymer-wrapped SWCNTs (SI3) is deposited onto the perovskite by spin-coating. Subsequently, a second layer of PMMA or undoped spiro-OMeTAD is deposited on top of the SWCNTs (Figure 1a) and b)).

The champion photovoltaic performance of both device types is shown in Figure 1c) and d), and Table 1. It is worth highlighting that the open-circuit voltage of the device is 1.192 V. Optical characterization of the absorber material allows us to measure the bandgap with a Tauc plot (Figure S2), from which we extract an optical bandgap of 1.57 eV. The Shockley-Queisser (SQ) limit for an absorber with this bandgap is $V_{oc}^{SQ} = 1.281$ V.[18] Notably, the V_{OC} of 1.192 V measured for the device utilizing the SWCNT/spiro-OMeTAD hole extraction layer translates to a very low voltage loss ($\Delta V_{OC} = V_{OC}^{SQ} - V_{OC}$) of 0.107 V. The condition required to achieve the SQ voltage limit (V_{OC}^{SQ}) is the prevention of all non-radiative recombination losses, so that at V_{OC}, an equal number of photons are absorbed as are emitted.[19] Non-radiative recombination losses occur for different reasons. At low charge carrier densities, non-radiative recombination is often mediated by trap states within the bulk of the absorber or at its surfaces. Another common cause for recombination is the interface between the absorber material and charge selective layers,[5,20,21] which can result from poor charge transport characteristics and the concomitant accumulation of charge at the interface.

Indeed, the performance of devices in which spiro-OMeTAD is replaced with an inert polymer, in this case PMMA, suggests that, interfacial recombination may be more prevalent when the SWCNTs constitute the only hole transport material. Figure 1c shows the champion current-

voltage curve of two devices with the different HTL configurations, and highlights the striking difference in the measured V_{OC}. The device with PMMA has a V_{OC} of 1.053 V, which is 0.139 V lower than for the device with spiro-OMeTAD. This indicates that in the absence of a complementary hole-transport material to accompany the SWCNTs, charges are likely to recombine at this interface much more readily. The overall trend is borne out in the device statistics (Figure 1 e) and f)), which show that the stabilized power output (SPO) is strongly correlated with the open-circuit voltage.

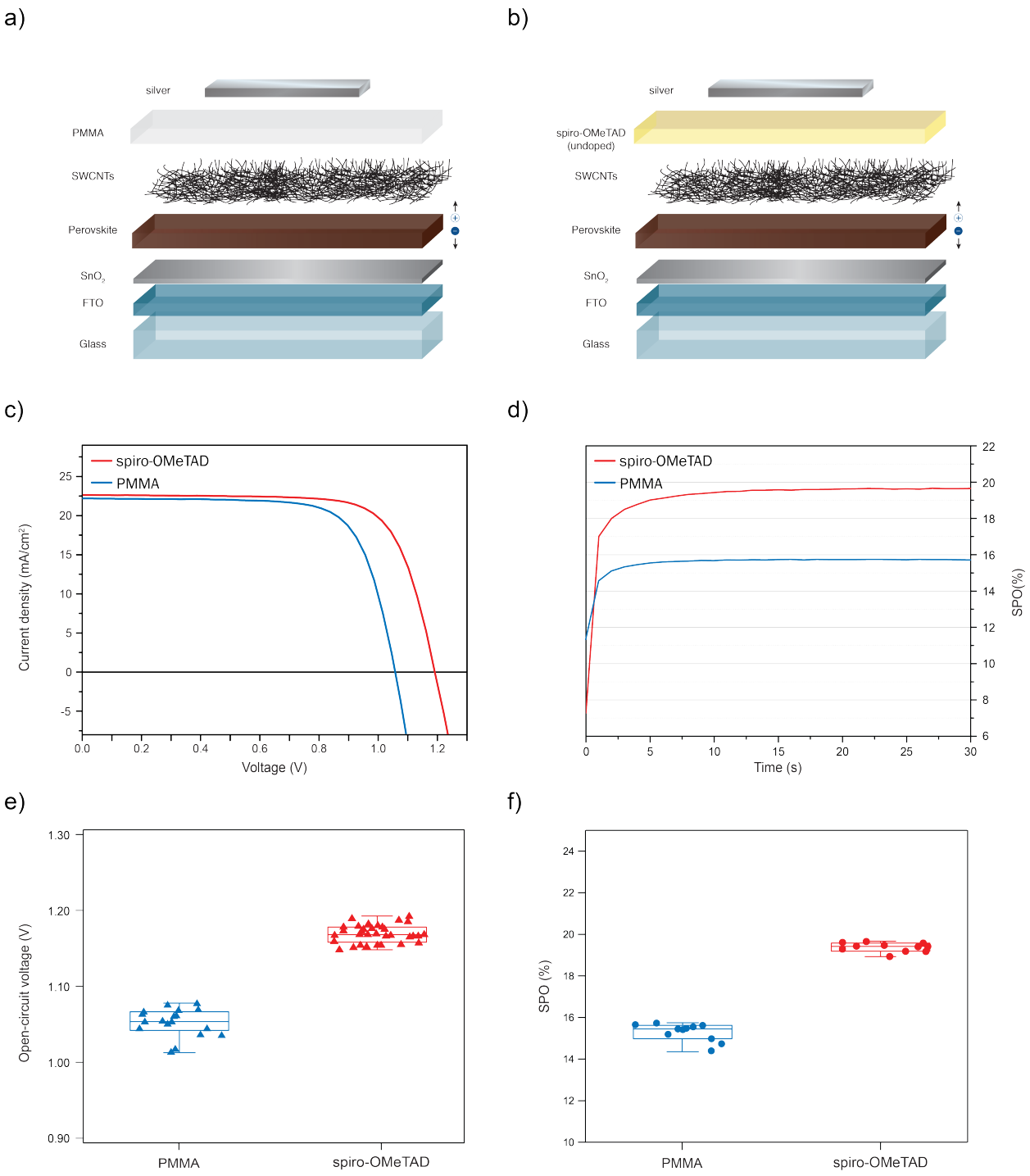

Figure 1: Schematics of the HTL configurations where the SWCNT matrix is encapsulated by a) PMMA (80 nm) and b) neat spiro-OMeTAD (350 nm). c) Current-voltage characteristics of two representative devices. d) The SPO values corresponding to the JV-scans in c). Statistical distribution of e) open-circuit voltages and f) SPO values.

Scan-dependent hysteresis in the current-voltage (JV) curves of perovskite solar cells results from the presence of mobile ions in the absorber and inhibited charge extraction at imperfect interfaces.[22,23] Changes to the internal field due to illumination and an external bias result in changes to the ion distribution in the perovskite absorber leading to a scan-direction dependent hysteresis in the JV-curves. While JV-scans can be highly instructive for device operation, determining the efficiency of a device unambiguously can only be done by letting the photocurrent stabilize over time when the device is held at its maximum power voltage. The SPO metric also provides insights into the steady-state distribution of mobile ions under device operating conditions.[22,23] The ratio of the scanned efficiency and the steady-state efficiency can thus be a proxy for the quality of the interfaces. For the device using PMMA as a top layer, the steady-state efficiency is 15.7% (figure 1c), table 1), and the ratio to the scanned efficiency is 0.90. This suggests that poling this device forward improves the charge extraction, likely due to ion accumulation at the interface. In contrast, the redistribution of the diffusing ions has a deleterious effect on the charge extraction and thus on the device performance. This is a further indication that extraction losses occur at the interface between the perovskite and the SWCNT+PMMA composite. In stark contrast, the SPO of the device with spiro-OMeTAD is 19.7%, thus having a ratio 0.99 to the scanned PCE. This exceptionally high stabilized power ratio (SPO/SPE) indicates much fewer extraction losses for the HTL configuration in which neat spiro-OMeTAD encases the thin SWCNT layer.

Table 1: Performance parameters of the champion devices using the two HTL configurations

HTL	J_{SC} [mA/cm^2]	V_{OC} [V]	FF	PCE [%]	SPO [%]	SPO/PCE
SWCNTs/PMMA (80 nm)	22.4	1.053	0.74	17.4	15.7	0.90
SWCNTs/spiro-OMeTAD (350 nm)	22.6	1.192	0.74	20.0	19.7	0.99

The field-independent charge extraction and the reduced voltage loss hint at an interesting synergistic effect of both the SWCNTs and the undoped spiro-OMeTAD layer at the perovskite interface, which results in effective charge extraction and a high open-circuit voltage. Since both JV curves have the same FF, we assume comparable parasitic resistance losses in both HTL configurations, so we can neglect them and express the V_{OC} with the ideal diode equation:

$$V_{\mathrm{OC}} \approx \frac{k_B T}{q} \ln\left(\frac{J_{\mathrm{SC}}}{J_0} + 1\right) \tag{1}$$

With both HTL configurations having similar J_{SC} values, the parameter determining the difference in V_{OC} is J_0, the dark saturation current. The dark-saturation current is a direct measure of the recombination rate in the device. In perovskite-based devices the majority of recombination events take place at the interfaces.[3,24] The implication is that while SWCNTs can, by themselves, effectively and selectively extract holes, they still appear to suffer from recombination losses

which can be minimized by the presence of a second material which can accept charges from the SWCNTs.

To test the hypothesis that the higher V_{OC} of the double layer of SWCNTs and neat spiro-OMeTAD can be attributed to fewer recombination losses, we investigate the effect of different HTL configurations on the recombination rate in the absence of an electron-transport layer (ETL). In the absence of an ETL all selective charge extraction must be ascribed to the quality of the HTL, such that the magnitude of J_0 measured in this configuration provides direct insight into the interfacial recombination dynamics. Specifically, in the absence of a selective contact, the recombination rate should be large and accordingly J_0 should be high, while the relative reduction of J_0 upon the introduction of a particular HTL indicates the relative degree to which recombination is suppressed.

Figure 2a shows J_0 for the bare perovskite absorber layer and the same absorber layer modified with three different HTLs. As expected, the magnitude of J_0 is highest for the bare absorber layer. With neat undoped spiro-OMeTAD, a dedicated hole-transport material can now selectively extract photogenerated holes and block electrons, which reduces recombination losses and, thus reduces J_0. The removal of charges from the perovskite is also reflected in a significant decrease in the photoluminescence (PL) lifetime compared to perovskite on glass without contacts (Figure 2b). It is important to note that PL lifetimes can be somewhat ambiguous for determining the fate of photogenerated charge carriers since they can only demonstrate changes in the lifetimes of radiatively recombining charges. They cannot be used by themselves to distinguish between the removal of charges due to selective extraction or increased non-radiative recombination. In our

case, they prove to be very useful in complementing the dark current measurements, which represent changes in the charge carrier recombination.

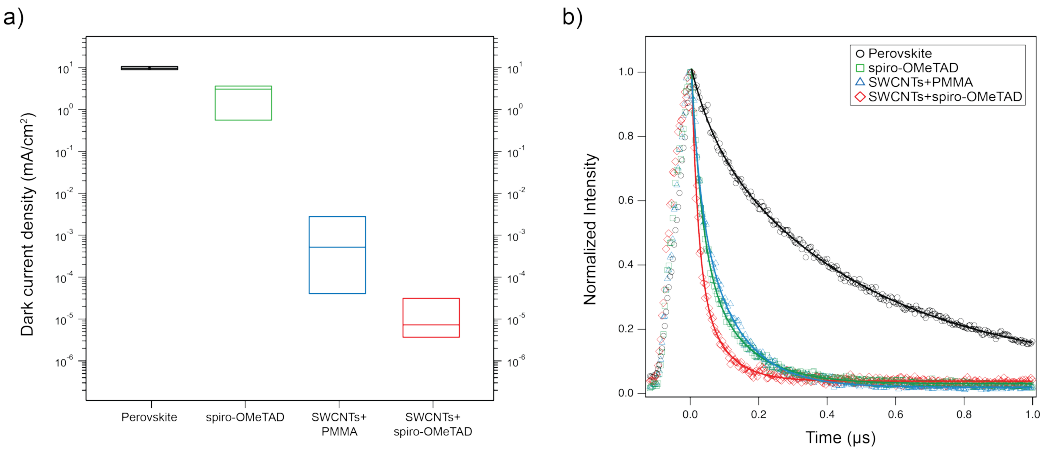

Figure 2. a) dark current values for different HTL configurations on device stack without electron-selective charge transport layer, b) time-resolved photoluminescence decays for different HTL configurations

Table 2. Average dark current values and photoluminescence lifetimes for different HTL configurations

	J_0 (mA/cm^2)	TRPL τ_{avg} (ns)
Perovskite	9.7	407
spiro-OMeTAD	3.1	70
SWCNTs+PMMA	$5.2 \cdot 10^{-4}$	81
SWCNTs+spiro-OMeTAD	$7.3 \cdot 10^{-6}$	40

The composite layer of SWCNTs with a PMMA matrix reduces J_0 by several orders of magnitude compared to neat undoped spiro-OMeTAD (Figure 2a, table 2), implying that even fewer charges are lost to recombination in this device. Interestingly, the PL lifetime is slightly longer, though comparable to that of neat spiro-OMeTAD. This observation indicates that for neat spiro-OMeTAD holes can rapidly transfer to the HTL, but still recombine across the interface giving

rise to significant J_0. In its undoped state, the hole mobility of spiro-OMeTAD is quite low.[25] As such, it seems likely that a relatively large hole population remains close to the interface long enough to recombine non-radiatively with electrons from the perovskite. Consistent with this interpretation, we find that solar cells with neat spiro-OMeTAD are limited by high series resistance (SI4). In the case of the SWCNT+PMMA layer, in contrast, the dark current is suppressed by several orders of magnitude, relative to the neat perovskite and the perovskite contacted with neat undoped spiro-OMeTAD. In this case, the holes rapidly transfer to the SWCNTs and then travel quickly through the SWCNTs to the electrode. However, the lowest J_0 is measured for the combination of SWCNTs at the interface and neat spiro-OMeTAD on top. In this case, the J_0 is another two orders of magnitude smaller due to the presence of the neat spiro-OMeTAD on top of the SWCNTs, an observation that is also consistent with this device having the shortest PL lifetime. From these observations, we conclude that photogenerated holes are extracted most effectively from the perovskite by the SWCNT+spiro-OMeTAD dual extraction layer without recombining.

The comparison between PMMA and spiro-OMeTAD as matrix on top of the SWCNTs, shows that the use of a hole-accepting material with the SWCNT extraction layer appears to be superior, because in its presence recombination is further suppressed. A conceivable mechanism for this observation could be a sequential transfer of holes. First, after photogeneration in the perovskite, holes are efficiently injected into the SWCNTs where they rapidly move away from the interface before they are transferred to the neat spiro-OMeTAD. At this point they are spatially removed from the interface to such a degree that they largely escape the fate of interfacial recombination.

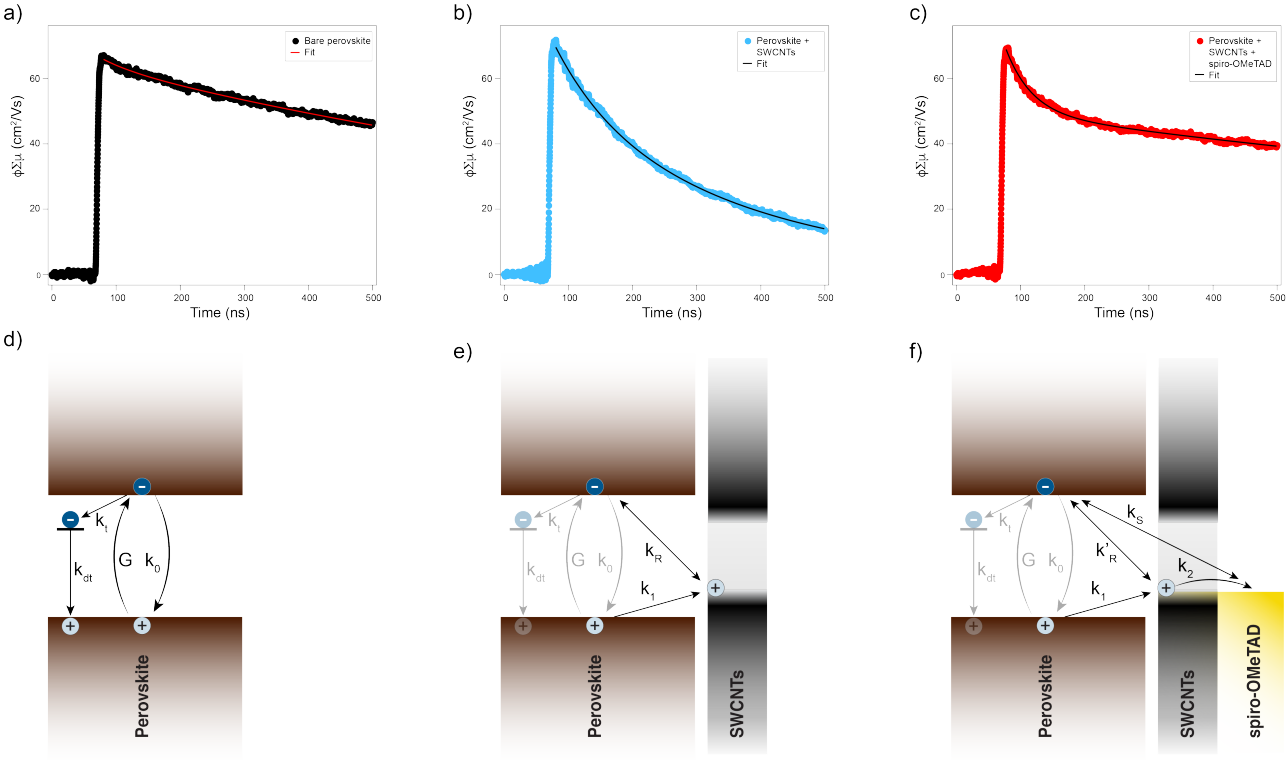

Figure 3. TRMC transients the same sample with sequential HTL depositions: bare perovskite a), perovskite with a thin layer of SWCNTs b), and perovskite with a thin layer of SWCNTs covered by a layer of undoped spiro-OMeTAD c), measured in an open-cell configuration at a pump wavelength of 640 nm and a fluence of 5 x 10^9 s^{-1}. The corresponding recombination schemes are shown in d)-f), respectively.

To further corroborate the notion of suppressed recombination in the presence of the secondary hole acceptor, we employ TRMC. TRMC is a contactless pump-probe technique that samples the generation and decay of photoexcited mobile charges by measuring the time-dependent attenuation of a GHz frequency microwave probe beam after an optical pump pulse has photogenerated charges in the absorber material.[26–28] The degree of microwave attenuation is proportional to the yield (ϕ) of photogenerated charges and their mobility (μ), which is described by a figure of merit

called the yield mobility product ($\phi\Sigma\mu$, where $\Sigma\mu = \mu_e + \mu_h$). Tracking this metric over time provides insight into the charge-carrier recombination and transfer dynamics.

The TRMC transients of various configurations were measured in an open-cavity configuration (Figure S6) and are shown in Figure 3, and the values of bi-exponential fits of the data are given in Table 3.

Table 3. Fitting parameters for a bi-exponential decay of the TRMC transients shown in Figure 3, providing the lifetimes and mobility values for the three different HTL configurations pumping at 640 nm and a fluence of 5 x 10^9

Fitting parameters	Perovskite	Perovskite+SWCNTs	Perovskite+SWCNTs+spiro-OMeTAD
A_1	2.7	21.3	20.0
τ_1 (ns)	45.3	87.8	40.8
A_2	63.4	48.8	49.4
τ_2 (ns)	1282.2	49.0	1845.7
$\Sigma\mu$ (Vs/cm^2)	**66.1**	**70.3**	**69.4**

The peak $\phi\Sigma\mu$ signal for the bare perovskite layer is relatively large ($\phi\Sigma\mu$ = 66.1 $cm^2V^{-1}s^{-1}$) and the decay is dominated by a long carrier lifetime of around 1200 ns (Figure 3a). Since the Coulomb attraction of charges in bulk (i.e. non quantum-confined) perovskite absorbers is heavily screened, we assume that photoexcitation produces all charges and no Coulomb-bound excitons (i.e. $\phi = 1$). Thus, the yield-mobility product $\phi\Sigma\mu$ reduces to the sum of the electron and hole mobilities in the perovskite layer ($\Sigma\mu$ = 66.1 $cm^2V^{-1}s^{-1}$). After the excitation pulse (G), the decay of the mobile

charge carriers (schematically shown in Fig. 3d) is exclusively determined by radiative band-to-band recombination (k_0) and non-radiative trap-mediated recombination (k_t, k_{dt}).

When the SWCNTs are deposited on the perovskite, the peak value of $\phi\Sigma\mu$ increases ($\phi\Sigma\mu$ = 70.3 $cm^2V^{-1}s^{-1}$) relative to the bare perovskite layer, and the dynamics of $\phi\Sigma\mu$ change significantly (Figure 3b). Previous time-resolved measurements suggest that the diffusion and transfer of photogenerated holes from the perovskite layer to the SWCNTs (k_1 in Figure 3e) should occur within the pulse of the TRMC pump (ca. 5 ns).[12] As such, the peak $\phi\Sigma\mu$ value, which again reduces to $\Sigma\mu$, is now defined by the electrons remaining in the perovskite and the holes that now reside in the SWCNT phase. Thus, the increased $\phi\Sigma\mu$ value observed for the 'perovskite + SWCNTs' sample suggests that the hole mobility of the SWCNT layer is slightly higher than the hole mobility within the perovskite layer. Following hole extraction by the SWCNTs, the signal decays rapidly due to charge recombination processes. The most likely recombination pathway is interfacial recombination (k_R, Figure 3e) in which the holes from the SWCNTs recombine with electrons in the perovskite.

Figure 3c shows the TRMC transient of the perovskite absorber modified with a layer of SWCNTs *and* undoped neat spiro-OMeTAD. The peak $\phi\Sigma\mu$ value is close to that of the 'perovskite + SWCNTs' sample ($\phi\Sigma\mu$ = 69.4 $cm^2V^{-1}s^{-1}$), suggesting that the initial signal immediately following the pulse is still dominated by holes in the SWCNTs and electrons in the perovskite layer. The signal decays with two distinct time constants, one fast and one much slower. The fast time constant we attribute to the transfer of holes from SWCNTs to the spiro-OMeTAD layer (k_2, Figure

3f) and the slow time constant we attribute to recombination between electrons in the perovskite and holes in the spiro-OMeTAD layer (k_S, Figure 3f). Due to the low mobility of holes in the spiro-OMeTAD layer, they are insufficiently mobile to affect the microwave pulse which makes them effectively invisible to detection in this measurement. As a consequence, as holes are transferred from the high-mobility SWCNT phase to the low-mobility spiro-OMeTAD layer, the signal decays. Following this initial decay, the remaining electrons within the perovskite layer are now the main contributors to the $\phi\Sigma\mu$ signal, which is now long-lived due to the reduced availability of recombination partners (the holes in the spiro-OMeTAD layer which are far spatially removed from the interface) and the consequently much slower interfacial recombination rate (k_S, Figure 3f)

The relatively large mobility value that we attribute to electrons remaining in the perovskite layer indicates that the $\phi\Sigma\mu$ signal within this perovskite absorber layer is dominated the mobility of electrons. We confirm this by contacting perovskite films with phenyl-C61-butyric acid methyl ester (PCBM), a well-known electron acceptor (Figure S7). The changes are qualitatively similar to the SWCNTs+spiro-OMeTAD contact, however, in contrast to the p-type contact, the mobility drops to 33% of the initial value. In this case, the photogenerated electrons were extracted from the perovskite absorber and the remaining signal can be attributed to the remaining holes in the perovskite. From this observation, we conclude that the electron mobility in this perovskite composition is more than twice as large than that of holes.

Based on these results we propose the following charge transfer mechanism for the perovskite+SWCNT+spiro-OMeTAD system: (i) photogenerated holes in the perovskite rapidly transfer to the SWCNTs (k_1), (ii) due to the presence of spiro-OMeTAD, the holes then undergo

another transfer to the secondary HTL (k_2), where (iii) they are long-lived due to spatial separation. As a consequence, back-transfer and interfacial charge recombination can be suppressed ($k'_R < k_S < k_R$), which eventually results in high photovoltages in solar cells.

This mechanism requires that the photogenerated holes transfer from the SWCNTs to the undoped spiro-OMeTAD prior to being collected by the electrode. One line of evidence that supports the proposed mechanism is the correlation between solar cell performance and the thickness of the undoped spiro-OMeTAD layer (Figure S8). The optimum spiro-OMeTAD layer thickness appears to be in the range of 320 nm at which the device performance peaks (Figure S8). Importantly, at the same PMMA thickness, PMMA-based devices do not function at all suggesting that at this thickness the SWCNTs are completely covered and do not make direct contact with the electrode. At a thickness of around 200 nm, a few SWCNTs can still penetrate the polymer layer thus yield functioning solar cells, however, at a strongly diminished performance (Figure S9). We thus infer an effective penetration thickness of the optimized SWCNT layer of around 200 nm. Limitations in the imaging techniques prevent us from directly imaging the penetration of the capping matrix by the SWCNTs (S10).

For thinner spiro-OMeTAD layers, the voltage is lower, while thicker layers have a decreased fill factor. This suggests that there are three regimes (illustrated in Figure S11): i) thick layers of undoped spiro-OMeTAD are increasingly series-resistance limited with thickness because of the increasing distance the holes have to traverse through the intrinsically low-conductivity material; ii) thin layers of spiro-OMeTAD allow for full SWCNT penetration, which now act as main hole-transporter but suffer from increased recombination resulting in voltage losses; iii) optimal layer

thickness, when the SWCNTs are fully covered, thus, holes have to transfer from the SWCNTs to a thin spiro-OMeTAD layer but where the short travel distance of the charges in this low-mobility layer does not contribute to an appreciably larger series resistance. Thus, these thickness-dependent data further support the importance of the charge transfer cascade from the SWCNTs to the capping layer in order to minimize recombination.

Complementary to this result is the observation, simultaneous optimization of the SWCNT layer thickness shows a similar trend with an optimal thickness (Figure S12). This optimum SWCNT thickness is presumably reached when the SWCNTs make a sufficient number contacts with the perovskite while also minimizing inter-tube junctions, which are known to inhibit charge transport, especially for junctions between semiconducting and metallic SWCNTs.[29]

While devices discussed thus far yield high photovoltages, they still suffer from some voltage loss relative to the ideal case. Therefore, the composite system of SWCNTs and undoped spiro-OMeTAD could conceivably still be a limiting factor with regards to the photovoltage. To demonstrate that, in fact, the main factor for voltage losses is the quality of perovskite absorber, we employ a method first demonstrated by Noel et al.,[30] where a small amount of formic acid (FAH) is added to the precursor solution which controls the size and concentration of colloids in the solution. The importance of the colloidal composition in the precursor for the quality of the perovskite film has previously been elucidated by McMeekin et al.[31]

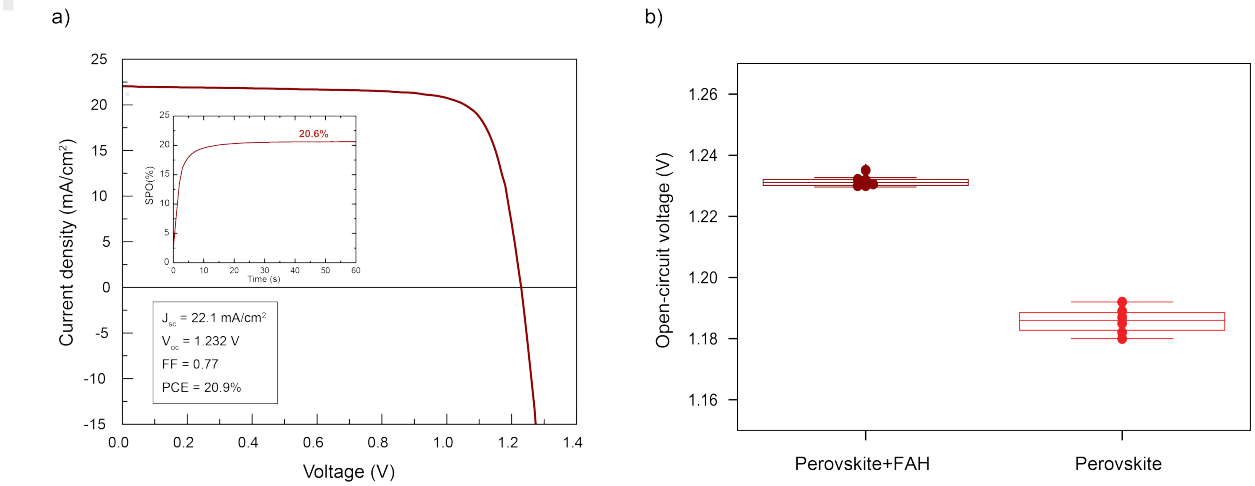

Figure 4: a) Current-voltage curve of a device with added formic acid to perovskite precursor with the steady-state efficiency as inset. b) V_{OC} comparison of perovskite with and without formic acid and the SWCNT/spiro-OMeTAD double layer HTL

The addition of a small amount of formic acid to our precursor solution yields a high-quality perovskite film which is characterized by fewer surface traps, and consequently fewer intrinsic non-radiative recombination losses at the interface, which was shown by a significant increase in the photoluminescence quantum efficiency to values exceeding 20%.[30]

When combined with the SWCNTs+spiro-OMeTAD double layer, the resulting champion device (**figure 4**) has an open-circuit voltage of 1.232 V at a bandgap of 1.57 eV (figure S13), for which the detailed balance limit predicts an open-circuit voltage of 1.281 V.[18] Consequently, the voltage loss in this device is merely 0.049 V, which is one of the lowest published voltage losses values achieved for a perovskite solar cell. With respect to the bandgap, the voltage loss is around 0.338 V which falls within the range of the highest quality semiconductors such GaAs (0.29 V) and GaInP (0.39 V).[32]

By comparing the charge-transfer interface between SWCNTs and perovskite in multiple different configurations, we can conclude that the charge transport characteristics of the charge-collecting layer is pivotal in order to achieve a high open-circuit voltage. The underlying mechanism is the reduction of interfacial recombination through the rapid spatial separation of charges at the perovskite-HTL interface via a cascade transfer mechanism.

The implication of our finding is that the development of new hole transport materials can have an additional degree of freedom by removing the need to include several orthogonal requirements, namely appropriate energetics, excellent kinetics and good barrier properties. We show, in particular, that the requirement for good charge transport properties at the interface can be outsourced to a separate material altogether.

In fact, our study suggests that the introduction of a rapid extraction interlayer may be sufficient to allow for low voltage losses, provided the secondary hole-accepting material is sufficiently charge-selective. It is conceivable that this finding holds true irrespective of the device architecture and the charge-selective contact, however, further research is necessary to confirm this notion. In particular, parallels might be drawn between the use of PCBM or C_{60} on the n-type side of perovskite devices as the rapid electron cascade initiator.[5]

Furthermore, in this double layer configuration, the intrinsic charge carrier mobility of the secondary material may not be as crucial for achieving high fill factors, as long as the mobility in the primary HTL is very high. Thus, the combination of the primary SWCNT extraction layer and secondary hole-transport material helps to relax the requirement of high charge carrier mobility in the secondary charge-selective contact, potentially allowing for a more targeted focus on

secondary hole-transport materials that improve stability. Crucial stability considerations to address include resilience against moisture ingress, structural integrity under thermal cycling, low oxygen permeability, UV stability, iodine impermeability and other essential properties to protect the perovskite absorber.[33] Generalizing these findings may be a crucial step for high-performance perovskite solar cells which are not limited by trade-offs between performance and stability.

Supporting Information

The Supporting Information is available free of charge on the ACS Publications website at DOI: XXXX.
Full experimental methods, device performance statistics, Tauc plot, SWCNT absorption, dark current plot, TRMC sensitivity calculations, PCBM TRMC transient, thickness dependencies, SEM cross section, PL of FAH modified perovskite.

Acknowledgements

J.L.B., O.G.R., and B.W.L. gratefully acknowledge funding from the Center for Hybrid Organic Inorganic Semiconductors for Energy (CHOISE), an Energy Frontier Research Center funded by the Office of Basic Energy Sciences, Office of Science, within the U.S. Department of Energy through contract number DE-AC36-08GO28308. S.N.H. was supported by the Director's Fellowship program of the National Renewable Energy Laboratory. The views expressed in the article do not necessarily represent the views of the DOE or the U.S. Government. The U.S. Government retains and the publisher, by accepting the article for publication, acknowledges that the U.S. Government retains a nonexclusive, paid-up, irrevocable, worldwide license to publish or reproduce the published form of this work, or allow others to do so, for U.S. Government purposes. N.K.N acknowledges funding from the Princeton Center for Complex Materials (PCCM).

(1) Kojima, A.; Teshima, K.; Shirai, Y.; Miyasaka, T. Organometal Halide Perovskites as Visible-Light Sensitizers for Photovoltaic Cells. *J. Am. Chem. Soc.* **2009**, *131* (17), 6050–6051.

(2) NREL. Best Research-Cell Efficiency Chart https://www.nrel.gov/pv/cell-efficiency.html

(accessed Jun 4, 2019).

(3) Braly, I. L.; DeQuilettes, D. W.; Pazos-Outón, L. M.; Burke, S.; Ziffer, M. E.; Ginger, D. S.; Hillhouse, H. W. Hybrid Perovskite Films Approaching the Radiative Limit with over 90% Photoluminescence Quantum Efficiency. *Nat. Photonics* **2018**, *12* (6), 355–361.

(4) Wong, K. K.; Fakharuddin, A.; Ehrenreich, P.; Deckert, T.; Abdi-Jalebi, M.; Friend, R. H.; Schmidt-Mende, L. Interface-Dependent Radiative and Nonradiative Recombination in Perovskite Solar Cells. *J. Phys. Chem. C* **2018**, *122* (20), 10691–10698.

(5) Fakharuddin, A.; Schmidt-Mende, L.; Garcia-Belmonte, G.; Jose, R.; Mora-Sero, I. Interfaces in Perovskite Solar Cells. *Adv. Energy Mater.* **2017**, *7* (22), 1700623.

(6) Stolterfoht, M.; Caprioglio, P.; Wolff, C. M.; Márquez, J. A.; Nordmann, J.; Zhang, S.; Rothhardt, D.; Hörmann, U.; Redinger, A.; Kegelmann, L.; et al. The Perovskite/Transport Layer Interfaces Dominate Non-Radiative Recombination in Efficient Perovskite Solar Cells. *arXiv Prepr. arXiv1810.01333* **2018**, *35* (5–6), 423–432.

(7) Schulz, P.; Cahen, D.; Kahn, A. Halide Perovskites: Is It All about the Interfaces? *Chem. Rev.* **2019**, *119* (5), 3349–3417.

(8) Dresselhaus, E. M. S.; Dresselhaus, G.; Avouris, P. Carbon Nanotubes; 2003; Vol. 4216, pp 329–391.

(9) Collins, P. G.; Bradley, K.; Ishigami, M.; Zettl, A. Extreme Oxygen Sensitivity of Electronic Properties of Carbon Nanotubes. *Science* **2000**, *287* (5459), 1801–1804.

(10) Habisreutinger, S. N.; Nicholas, R. J.; Snaith, H. J. Carbon Nanotubes in Perovskite Solar Cells. *Adv. Energy Mater.* **2017**, *7* (10), 1601839.

(11) Schulz, P.; Dowgiallo, A.-M.; Yang, M.; Zhu, K.; Blackburn, J. L.; Berry, J. J. Charge Transfer Dynamics between Carbon Nanotubes and Hybrid Organic Metal Halide

Perovskite Films. *J. Phys. Chem. Lett.* **2016**, *7* (3), 418–425.

(12) Ihly, R.; Dowgiallo, A.-M.; Yang, M.; Schulz, P.; Stanton, N. J.; Reid, O. G.; Ferguson, A. J.; Zhu, K.; Berry, J. J.; Blackburn, J. L. Efficient Charge Extraction and Slow Recombination in Organic-Inorganic Perovskites Capped with Semiconducting Single-Walled Carbon Nanotubes. *Energy Environ. Sci.* **2016**, *9* (4), 1439–1449.

(13) Jeon, I.; Matsuo, Y.; Maruyama, S. Single-Walled Carbon Nanotubes in Solar Cells. *Top. Curr. Chem.* **2018**, *376* (4), 1–28.

(14) Jeon, I.; Xiang, R.; Shawky, A.; Matsuo, Y.; Maruyama, S. Single-Walled Carbon Nanotubes in Emerging Solar Cells: Synthesis and Electrode Applications. *Adv. Energy Mater.* **2018**, *1801312*, 1–27.

(15) Lee, J.-W.; Jeon, I.; Lin, H.-S.; Seo, S.; Han, T.-H.; Anisimov, A.; Kauppinen, E. I.; Matsuo, Y.; Maruyama, S.; Yang, Y. Vapor-Assisted Ex-Situ Doping of Carbon Nanotube toward Efficient and Stable Perovskite Solar Cells. *Nano Lett.* **2019**, *19* (4), 2223–2230.

(16) Habisreutinger, S. N.; Leijtens, T.; Eperon, G. E.; Stranks, S. D.; Nicholas, R. J.; Snaith, H. J. Enhanced Hole Extraction in Perovskite Solar Cells Through Carbon Nanotubes. *J. Phys. Chem. Lett.* **2014**, *5* (23), 4207–4212.

(17) Habisreutinger, S. N.; Wenger, B.; Snaith, H. J.; Nicholas, R. J. Dopant-Free Planar n–i–p Perovskite Solar Cells with Steady-State Efficiencies Exceeding 18%. *ACS Energy Lett.* **2017**, *2* (3), 622–628.

(18) Rühle, S. Tabulated Values of the Shockley–Queisser Limit for Single Junction Solar Cells. *Sol. Energy* **2016**, *130*, 139–147.

(19) Tress, W. Perovskite Solar Cells on the Way to Their Radiative Efficiency Limit – Insights Into a Success Story of High Open-Circuit Voltage and Low Recombination. *Adv.*

Energy Mater. **2017**, *7* (14), 1602358.

(20) Stranks, S. D. Nonradiative Losses in Metal Halide Perovskites. *ACS Energy Lett*. **2017**, *2* (7), 1515–1525.

(21) Stolterfoht, M.; Wolff, C. M.; Márquez, J. A.; Zhang, S.; Hages, C. J.; Rothhardt, D.; Albrecht, S.; Burn, P. L.; Meredith, P.; Unold, T.; et al. Visualization and Suppression of Interfacial Recombination for High-Efficiency Large-Area Pin Perovskite Solar Cells. *Nat. Energy* **2018**, *3* (10), 847–854.

(22) Habisreutinger, S. N.; Noel, N. K.; Snaith, H. J. Hysteresis Index: A Figure without Merit for Quantifying Hysteresis in Perovskite Solar Cells. *ACS Energy Lett*. **2018**, *3* (10), 2472–2476.

(23) Tress, W. Metal Halide Perovskites as Mixed Electronic–Ionic Conductors: Challenges and Opportunities—From Hysteresis to Memristivity. *J. Phys. Chem. Lett*. **2017**, *8* (13), 3106–3114.

(24) Noel, N. K.; Abate, A.; Stranks, S. D.; Parrott, E. S.; Burlakov, V. M.; Goriely, A.; Snaith, H. J. Enhanced Photoluminescence and Solar Cell Performance via Lewis Base Passivation of Organic–Inorganic Lead Halide Perovskites. *ACS Nano* **2014**, *8* (10), 9815–9821.

(25) Leijtens, T.; Lim, J.; Teuscher, J.; Park, T.; Snaith, H. J. Charge Density Dependent Mobility of Organic Hole-Transporters and Mesoporous TiO_2 Determined by Transient Mobility Spectroscopy: Implications to Dye-Sensitized and Organic Solar Cells. *Adv. Mater*. **2013**, *25* (23), 3227–3233.

(26) Reid, O. G.; Moore, D. T.; Li, Z.; Zhao, D.; Yan, Y.; Zhu, K.; Rumbles, G. Quantitative Analysis of Time-Resolved Microwave Conductivity Data. *J. Phys. D. Appl. Phys*. **2017**,

50 (49), 493002.

(27) Savenije, T. J.; Ferguson, A. J.; Kopidakis, N.; Rumbles, G. Revealing the Dynamics of Charge Carriers in Polymer:Fullerene Blends Using Photoinduced Time-Resolved Microwave Conductivity. *J. Phys. Chem. C* **2013**, *117* (46), 24085–24103.

(28) Warman, J. M. Time Resolved Conductivity Techniques, DC to Microwave. In *Pulse Radiolysis of Irradiated Systems*; Tabata, Y., Ed.; CRC Press: Boca Raton, 1991; pp 101–133.

(29) Fuhrer, M. S.; Nygård, J.; Shih, L.; Forero, M.; Yoon, Y.-G.; Choi, H. J.; Ihm, J.; Louie, S. G.; Zettl, A.; McEuen, P. L. Crossed Nanotube Junctions. *Science* **2000**, *288* (5465), 494–497.

(30) Noel, N. K.; Congiu, M.; Ramadan, A. J.; Fearn, S.; McMeekin, D. P.; Patel, J. B.; Johnston, M. B.; Wenger, B.; Snaith, H. J. Unveiling the Influence of PH on the Crystallization of Hybrid Perovskites, Delivering Low Voltage Loss Photovoltaics. *Joule* **2017**, *1* (2), 328–343.

(31) McMeekin, D. P.; Wang, Z.; Rehman, W.; Pulvirenti, F.; Patel, J. B.; Noel, N. K.; Johnston, M. B.; Marder, S. R.; Herz, L. M.; Snaith, H. J. Crystallization Kinetics and Morphology Control of Formamidinium–Cesium Mixed-Cation Lead Mixed-Halide Perovskite via Tunability of the Colloidal Precursor Solution. *Adv. Mater.* **2017**, *29* (29), 1607039.

(32) Nayak, P. K.; Mahesh, S.; Snaith, H. J.; Cahen, D. Photovoltaic Solar Cell Technologies: Analysing the State of the Art. *Nat. Rev. Mater.* **2019**, *4* (4), 269–285.

(33) Christians, J. A.; Habisreutinger, S. N.; Berry, J. J.; Luther, J. M. Stability in Perovskite Photovoltaics: A Paradigm for Newfangled Technologies. *ACS Energy Lett.* **2018**, *3* (9),

2136–2143.